Resilience-Oriented Computationally Intensive Operation of Renewable-Powered Reconfigurable Microgrids: A Matheuristic Approach

Seyed Farhad Zandrazavi, *Member, IEEE*, Juan M. Home-Ortiz, and Miadreza Shafie-khah, *Senior Member, IEEE*

***Abstract*—This paper addresses the challenge of achieving both sustainability and resilience in renewable-powered reconfigurable microgrids (RMGs) while managing computational burdens. The Green Independence Performance Index (GIPI) is introduced as a novel resilience metric designed to maximize microgrid independence from the utility grid while avoiding renewable energy curtailment. A multi-objective, nonlinear, and non-convex optimization model is developed to simultaneously minimize total operational costs and maximize GIPI. To enhance tractability and guarantee solution optimality, the problem is reformulated as a mixed-integer linear programming (MILP) model using piecewise linearization and approximation techniques. To further reduce computational burden, a custom matheuristic algorithm is introduced, which synergistically combines classical MILP optimization with a neighborhood-structure-based heuristic. Numerical experiments on the enhanced IEEE 33-bus benchmark system demonstrate that the proposed GIPI eliminates renewable energy curtailment, unlike the IPI which curtailed 13.58% of photovoltaic and 25.09% of wind generation, while the proposed matheuristic reduces computational time from 1,629.74 s (CPLEX) to only 103.32 s and maintains near-optimal operating costs.**

***Index Terms*—Energy curtailment, matheuristic, reconfigurable microgrid (RMG), renewable energy, resilience, sustainability.**

NOMENCLATURE

Abbreviations

DG	Distributed generation.
DER	Distributed energy resource.
GIPI	Green Independence Performance Index.
IPI	Independence Performance Index.
MG	Microgrid.
MILP	Mixed-integer linear programming.
MINLP	Mixed-integer nonlinear programming.
OF	Objective function.
PV	Photovoltaic.
RMG	Reconfigurable microgrid.
RPC	Reactive power compensator.

Indices and sets

ω, Φ_ω	Index & set for blocks in piecewise linearization.
b, Φ_b	Index & set for battery.
dg, Φ_{dg}	Index & set for distributed generation.
$k,\ m,\ n,\ \Phi_N$	Index & set for node.
$km,\ mn,\ \Phi_L$	Index & set for line.
pv, Φ_{pv}	Index & set for photovoltaic unit.
t, Φ_T	Index & set for time interval.
w, Φ_w	Index & set for wind turbine unit.

Parameters

Δ_t	Duration of time interval [h].
Ψ^b_{dg}, Ψ^C_{dg}	Cost coefficients of DG [USD/kWh], [USD/(kWh)2].
Ψ^{GRb}_t, Ψ^{GRs}_t	Electricity price (buy/sell) [USD/kWh].
η^C_b, η^D_b	Charging/Discharging efficiency of battery.
E^{ini}_b	Initial level of energy in battery [kWh].
$E^{\max}_b$, E^{min}_b	Maximum/Minimum energy level of battery [kWh].
$I^{\max}_{mn}$	Maximum current flowing in line [A].
$\bar{\omega}$	Number of pieces in piecewise linearization.
$M^{PQ}_{mn,\omega}$	Slope in piecewise linearization of power flow.
$M^{DG}_{dg,\omega}$	Slope in piecewise linearization of DG's power.
P^{Cmax}_b, P^{Dmax}_b	Maximum charging/discharging power of battery [kW].
$P^{\max}_{dg}$, P^{min}_{dg}	Maximum/Minimum power of DG units [kW].

Received 6 July 2025; revised 5 October 2025; accepted 20 November 2025. Date of publication 15 January 2026; date of current version 20 July 2026. Paper 2025-SECSC-0898.R1, presented at the Commercial Power Systems Europe, Rome, Italy, Jun. 17–20, and approved for publication in the IEEE TRANSACTIONS ON INDUSTRY APPLICATIONS by the Renewable and Sustainable Energy Conversion Systems Committee of the IEEE Industry Applications Society [DOI: 10.1109/EEEIC/ICPSEurope61470.2024.10750960]. This work was supported by TotalEnergies EP Brazil through the ANP Regulatory Incentive for R&D. *(Corresponding author: Seyed Farhad Zandrazavi.)*

Seyed Farhad Zandrazavi is with the Electrical Engineering Team, School of Technology and Innovations, University of Vaasa, 65200 Vaasa, Finland (e-mail: seyed.zandrazavi@uwasa.fi).

Juan M. Home-Ortiz is with the Department of Systems and Energy, University of Campinas, São Paulo 13083-852, Brazil (e-mail: jumaho@unicamp.br).

Miadreza Shafie-khah is with Research and Innovation Division, Nowocert, D07 WP89 Dublin, Ireland (e-mail: miadreza@ieee.org).

Color versions of one or more figures in this article are available at https://doi.org/10.1109/TIA.2026.3654041.

Digital Object Identifier 10.1109/TIA.2026.3654041

$\widetilde{P_{pv,t}^{PV}}$, $\widetilde{P_{wt,t}^{WT}}$	Available PV and wind power generation [kW].
$P_{m,t}^{Load}$, $Q_{m,t}^{Load}$	Active/reactive power load [kW], [kVar].
$P_{GR}^{\max}$	Maximum power exchanged between MG & grid [kW].
Q_{rpc}^{RPC}	Reactive power injected by RPC [kVar].
φ_{dg}^{DG}	Power factor of distributed generation units.
R_{mn}, X_{mn}, Z_{mn}	Resistance, reactance, impedance of lines [ohm].
$V_m^{\max}$, V_m^{min}	Maximum/ Minimum voltage magnitude [kV].
V_n^{Esqr}	Estimation for square of voltage [(kV)^2].

Variables

$e_{b,t}^B$	Energy stored in battery [kWh].
$i_{mn,t}$	Current flowing in lines [A].
$i_{mn,t}^{sqr}$	Square of current flowing in lines [A^2].
$\Delta p_{mn,t,\omega}$,$\Delta q_{mn,t,\omega}$	Block of active/reactive power flowing in lines [kW], [kVar].
$p_{mn,t}$, $q_{mn,t}$	Active/reactive power flowing [kW], [kVar].
$p_{mn,t}^{+}$, $q_{mn,t}^{+}$	Active/reactive power flowing in lines (forward direction) [kW], [kVar].
$p_{mn,t}^{-}$, $q_{mn,t}^{-}$	Active/reactive power flowing in line (backward direction) [kW], [kVar].
$p_{b,t}^B$	Power of battery [kW].
$p_{b,t}^C$, $p_{b,t}^D$	Charging/discharging power of battery [kW].
$p_{dg,t}^{DG}$, $q_{dg,t}^{DG}$	Active/reactive power of DG units [kW], [kVar].
p_t^{GR}, q_t^{GR}	Active/reactive power exchanged with grid [kW], [kVar] .
$p_{pv,t}^{PV}$, $p_{w,t}^{W}$	Actual PV& wind power injection [kW].
$p_{pv,t}^{Cut}$, $p_{w,t}^{Cut}$	Active power curtailments [kW].
$\Gamma_{mn,t}$	Auxiliary free variable .
$v_{m,t}$	Voltage magnitude [kV].
$v_{m,t}^{sqr}$	Square of voltage magnitude [(kV)^2].
$y_{mn,t}^{-}$, $y_{mn,t}^{+}$	Binary variables to model status of line.
δ_t^{GRb}, δ_t^{GRs}	Binary variables for selling/buying status of MG.

I. Introduction

A. Motivation & Background

MICROGRIDS (MGs) play a key role in transitioning from centralized, fossil fuel-based generation to decentralized, renewable energy-powered systems by supporting the adoption of electric vehicles (EVs) and distributed energy resources (DERs) [1]. MGs are expected to experience substantial growth in the coming years, particularly in the Asia-Pacific and North American regions [2]. By 2027, both annual capacity installations and investments are expected to be five times higher than they were in 2018 [2]. Achieving zero or near-zero carbon emissions in main grids is challenging due to high costs and low reliability with high renewable integration and large-scale storage. However, zero-carbon MGs are more feasible due to their smaller scale [3]. Nevertheless, the advantages of MGs are not limited to decarbonization, as MGs have considerable flexibility resources and can provide various ancillary services for the main grid improving security, reliability, and resilience.

The concept of resilience has been widely considered in the modern power system planning, operation, and control [4]. Past events have highlighted the important role of MGs in strengthening energy resilience. For example, during the 2011 Tohoku earthquake in Japan, the Sendai MG continued to provide both electricity and heat to its users [5]. Similarly, after Superstorm Sandy in 2012, the MG at the U.S. Food and Drug Administration's White Oak Research Facility in Maryland successfully disconnected from the main grid and supplied local loads [5]. These cases illustrate the capability of MGs to maintain energy supply during severe natural disasters. Although resilience is widely recognized as a key concept in modern power systems, a universally accepted definition has not yet been established, as interpretations often differ [6]. In general, resilience refers to the ability of power systems to anticipate, withstand, adapt to, and recover from disruptive events, covering both physical infrastructure and operational continuity [6]. To distinguish it from reliability, resilience is usually described as focusing on high-impact, low-probability disturbances, while reliability addresses low-impact, high-probability events [7]. This broad interpretation of resilience has led to the development of various resilience indices. For instance, [8] defines three different measures for enhancing MG resilience. The first seeks to reduce dependence on the utility grid, ensuring that MGs can operate during contingencies or unintentional islanding. The second maximizes the use of hydrogen reserves that can be converted into electricity when the utility grid is disrupted. The third applies the classical power loss minimization as a resilience metric [8]. In a similar way, [9] introduces the Independence Performance Index (IPI), which improves MG resilience by reducing purchased power and increasing independence from the utility. Such broad and evolving perspectives on resilience in power systems, and particularly in MGs, are valuable given the novelty of the concept. However, our case studies indicate that these indices must be defined and applied carefully, as some may result in unintended consequences.

In distribution networks, reconfiguration plays a key role in service restoration and enhancing resiliency against faults, extreme weather events, and cyber-physical threats [10]. Network reconfiguration involves modifying the topological structure of a power system by opening or closing switches to achieve either a radial or meshed configuration [11]. Its application extends beyond MG formation, since it is widely used to minimize losses, improve load balancing, enhance voltage profiles, reduce costs, and increase overall system reliability in distribution networks [12]. Incorporating network reconfiguration introduces a large number of binary variables to represent the status of each line (i.e., open or closed), which has led to the widespread use of metaheuristic optimization in this context [13]. Nevertheless, matheuristic methods can perform better than pure metaheuristics as they use exact mathematical optimization to guide the heuristic search more effectively [14]. This allows them to find higher-quality solutions faster, even with large-scale problems with many binary variables [14]. In other words, they balance the strengths of exact mathematical methods and heuristics, giving accurate results without excessive computation.

Considering the importance of both resilience and reconfigurability in MGs, it is crucial to study the resilience-oriented operation of reconfigurable microgrids (RMGs) in the presence of renewable energy generation.

B. Literature Review

This section reviews recent key papers on RMG and resilient operation of MGs to properly highlight the research gap and underscore contributions of this study.

A significant number of studies is available on RMGs in the literature, typically to minimize the power loss, total cost, and improve the voltage profile of the system. In [15], a chance-constrained optimization model for the optimal operation of RMGs is proposed to ensure reliable islanded operation. An energy trading framework for RMG is introduced in [16] to optimize the cost, efficiency, and grid stability. The results show that demand response and network reconfiguration lead to a considerable reduction in trading costs. An energy management system for a hybrid AC/DC RMG is introduced in [17] to minimize electricity costs and improve the reliability of the system. The method dynamically reconfigures MGs based on load and renewable energy forecasts, showing significant cost reductions and performance improvements [17]. In [18], a hybrid blockchain and stochastic programming framework for the optimal scheduling of reconfigurable multi-MGs is proposed to reduces operational costs and enhances energy supply reliability. A privacy-preserving distributed control strategy for the optimal economic operation of islanded RMG is reported in [19] to enhance the operational flexibility. As EVs may increase power losses and cause feeder overloading, a data-driven stochastic optimization model is proposed for the optimal operation of RMGs in [20]. This model not only utilizes reconfigurability to mitigate these negative effects but also handles the uncertainties associated with EVs [20]. In [21], a multi-objective model for optimal operation of RMG is presented to minimize voltage deviation (i.e., improve voltage profile) and the total cost. A stochastic profit-based day-ahead scheduling framework for RMGs is suggested in [22] and a time-varying acceleration coefficients particle swarm optimization algorithm is employed to determine the optimal topology, unit dispatch, and power exchange with the main grid [22]. In [23], a multi-objective stochastic scheduling is proposed for RMG to minimize operational costs and carbon emissions while enhancing system flexibility and reliability. An optimization model is developed in [24] for optimal day-ahead scheduling of a hybrid RMG with responsive demand to enhance stability, reduce operational costs, and improve power quality. In [25], an optimization model for the optimal operation of islanded RMGs is presented by focusing on P-Q capability curves of DGs. The presented model aims to minimize total system power loss, while a set of operational constraints are included. In [26], a stochastic MILP optimization model is proposed for the energy management of hybrid AC/DC MGs, incorporating dynamic line rating (DLR). Network reconfiguration is employed to modify the network topology and mitigate line congestion caused by DLR limitations, particularly in islanded mode.

Resilient operation of MGs attracted more researchers during the last decade. A profound review of the resilience in power systems and MGs is provided in [6]. In [8], a multi-objective resilience-based model for optimal operation of MGs incorporating power-to-hydrogen systems is proposed. The presented model enables flexible hydrogen utilization for electricity generation or industrial purposes [8]. A two-stage stochastic optimization model is proposed for resilient operation of unbalanced islanded MGs, considering uncertainties in demand, renewable generation, and voltage reference at the point of common coupling [27]. An energy management optimization model is developed and tested for multicarrier MGs in [28] to enhance resilience against power outages and to minimize operational costs. In [29], a multi-objective optimization model for the optimal scheduling of MGs is proposed to minimize operational cost and emissions, while maximizing resilience, highlighting the role of EVs. A hybrid stochastic-robust optimization model for resilient operation of MGs including demand response and uncertainty modeling is developed in [30]. In [31], a convex optimization model is proposed to enhance the resilience of MGs by taking some preventive measures such as prioritizing critical loads and decreasing the dependency on generators with higher risk of failure. In [32], the potential of battery electric buses as a resiliency resource for islanded MGs during grid outages is analyzed. The findings highlight that electric buses can support critical loads, provide black start capability, and enhance the overall flexibility and resilience of islanded MGs [32]. A multi-objective optimization framework is developed in [33] for the optimal operation of a hydrogen-electricity coupled MG. The focus is on balancing economic efficiency with resilience to external grid disruptions, ensuring continuous operation of critical loads [33]. A two-stage robust day-ahead optimization model for MGs considering demand response and voltage regulation is presented in [34] to minimize operating costs while ensuring resilient operation. In [35], resilience in the optimal operation of MGs is addressed through islanding capability, which requires MGs to sustain their local loads during any possible outage of predefined consecutive hours within the scheduling horizon.

While service restoration in distribution networks through MG formation has been widely explored in the literature [36], limited studies focus on the resilience operation of MGs considering reconfiguration. To improve the resilience of islanded RMGs, an optimization method is reported in [37] to ensures the smooth operation of MGs in both economic mode (under normal conditions) and resilience mode (before low-probability high-impact events). In [38], a robust two-stage optimization model is presented to minimize the total cost and power loss in RMG, while including uncertainties related to renewable generation and load demand. In [39], a framework for selecting best topologies to enhance resilience in islanded MGs is presented. The framework integrates optimal asset positioning, stability assessment, and resilience quantification to identify fault-tolerant network designs that enhance system resilience and performance. Despite their contributions, these studies overlooked the computational complexity of reconfiguration as well as the importance of renewable energy curtailment.

C. Contribution

In existing literature, many valuable studies have explored the operation of RMGs. However, most have focused either on cost minimization, emission mitigation or technical indices such as voltage deviation and power loss reduction, overlooking the importance of resilience. Some studies have examined the resilient operation of MGs but have not explored the potential of reconfiguration. Others that address resilience-oriented operation in RMGs overlooked the computational complexity and the integration of renewable generation in resilience indices. Therefore, to the best of the authors' knowledge, a comprehensive model that fully incorporates resilience-oriented operation and MG reconfigurability while addressing renewable energy curtailment and the computational complexity associated with a large number of binary variables is still lacking in the current literature. This study substantially expands upon our previous research presented in [40]. The contributions of this study can be summarized as follows:

1) Development of a multi-objective optimization model for renewable-powered reconfigurable microgrids that introduces a new sustainability-driven resilience metric, the Green Independence Performance Index. This model integrates sustainability directly into the resilience objective by maximizing grid independence, while avoiding renewable energy curtailment.
2) Design and implement of a custom matheuristic optimization approach to efficiently solve the proposed computationally intensive mathematical model, where the multi-objective optimization problem is tackled by solving derived subproblems of the MILP model using a commercial solver, with the obtained solutions serving as neighborhood structures in the VND metaheuristic framework.

II. Mathematical Formulation

In this research, the main goal of the RMG is to minimize the total operational cost while maximizing the Green Independence Performance Index (GIPI). In the following subsections, more details regarding objective functions and technical constraints are provided.

A. Objective Function

The proposed model's first objective function (OF_1) is to minimize the operational cost of the RMG during the operating horizon, as expressed in (1). The first part addresses the cost of energy which is exchanged between the MG and the main grid. More specifically, p_t^{GRb} indicates that power is imported (bought) from the grid, representing a cost. Conversely, p_t^{GRs} indicates that power is exported (sold) to the main grid, generating revenue for the MG. A quadratic function is often used to model the cost of generating electricity from distributed generation (DG) units because it captures the relationship between the output power and the increasing marginal costs as generation increases. Thus, the second term in (1) represents the cost function of DG units.

$$OF_1 = \min \left(\begin{array}{l} \sum_t \Delta_t \left(\Psi_t^{GRb} p_t^{GRb} - \Psi_t^{GRs} p_t^{GRs} \right) \\ + \left(\sum_t \sum_{dg} \Delta_t p_{dg,t}^{DG} \Psi_{dg}^{b} + \left(\Delta_t p_{dg,t}^{DG} \right)^2 \Psi_{dg}^{C} \right) \end{array} \right) \tag{1}$$

Independence Performance Index (IPI) is introduced in [41] by Karimi and Jadid as shown in (2), to enhance resilience of MG by maximizing the independence of the MG from the main grid, where $P_{m,t}^{Load}$ represents the active power demand. In this index, the independence can be defined based on the proportion of power received from the main grid and the total electric loads as presented in (2). However, in this research, the proposed index for resilience is adjusted to include environmental concerns and renewable energy curtailment. Therefore, (2) is modified to (3), by adding the generation from photovoltaic and wind turbine units to the IPI. In this modified index, MG aims to increase resilience, while ensuring that renewable energy generation is not compromised. As a result, a novel resilience index, the GIPI, is proposed and considered as the second objective function (OF_2), as presented in (3). In GIPI, a new term which is the proportion of renewable energy generation compared to the total load is added to the IPI metric.

$$IPI = \text{Max} \left(1 - \frac{\sum_t p_t^{GRb}}{\sum_t \sum_m P_{m,t}^{Load}} \right) \tag{2}$$

$$OF_2\,(GIPI) = \text{Max} \left(1 - \frac{\sum_t \left(p_t^{GRb} \right)}{\sum_t \sum_m P_{m,t}^{Load}} + \frac{\sum_t \sum_w p_{w,t}^{W} + \sum_t \sum_{pv} p_{pv,t}^{PV}}{\sum_t \sum_m P_{m,t}^{Load}} \right) \tag{3}$$

$$p_t^{GR} = p_t^{GRb} - p_t^{GRs};\ \forall t \in \Phi_T \tag{4}$$

$$p_t^{GRb} \le \delta_t^{GRb} P_{GR}^{\max};\ \forall t \in \Phi_T \tag{5}$$

$$p_t^{GRs} \le \delta_t^{GRs} P_{GR}^{\max};\ \forall t \in \Phi_T \tag{6}$$

$$\delta_t^{GRb} + \delta_t^{GRs} \le 1;\ \forall t \in \Phi_T \tag{7}$$

B. Day-Ahead Non-Linear Non-Convex Optimization Model

The secure operation of the MG necessitates satisfying technical constraints, such as voltage and current magnitude limits, to meet operational challenges. In the day-ahead scheduling, the active and reactive power generation, battery charging/discharging [42], the status of tie-line switches (i.e., open or closed) [43], and the amount of renewable energy curtailment [44] will be determined. To facilitate understanding of power balance and AC power flow, a simple 3-bus illustrative example is presented in Fig. 1.

1) Power Balance: The balance of active and reactive power at each node and time interval is maintained through equality constraints (8) and (9) [45]. In (8), the left-hand side represents the injected active power from the grid, DG units, and renewable

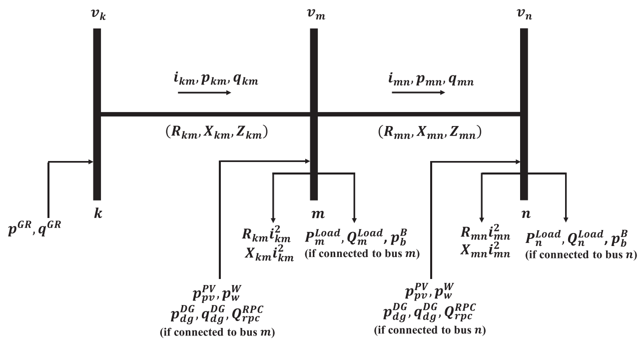

Fig. 1. A simplified illustrative example of a 3-bus system for AC power flow.

sources, while the right-hand side reflects the absorbed active power related to battery charging and active power demands. Similarly, (9) considers reactive power generation from the grid, reactive power compensators (RPC), and DG units on the left-hand side, while the right-hand side captures the reactive power demand.

$$\sum_{km} p_{km,t} - \sum_{mn} \left(p_{mn,t} + R_{mn} i^2_{mn,t}\right) + \sum_{dg|\ b_{dg}=\ m} p^{DG}_{dg,t} + \sum_{pv|\ b_{pv}=\ m} p^{PV}_{pv,t} + \sum_{w|\ b_w=\ m} p^{W}_{w,t} + p^{GR}_t = P^{Load}_{m,t} + \sum_{b|\ b_b=\ m} p^{B}_{b,t};\ \forall m \in \Phi_N, \forall t \in \Phi_T \tag{8}$$

$$\sum_{km} q_{km,t} - \sum_{mn} \left(q_{mn,t} + X_{mn} i^2_{mn,t}\right) + \sum_{dg|\ b_{dg}=\ m} q^{DG}_{dg,t} + \sum_{rpc|\ b_{rpc}=\ m} Q^{RPC}_{rpc} + q^{GR}_t = Q^{Load}_{m,t}\ ;\ \forall m \in \Phi_N, \forall t \in \Phi_T \tag{9}$$

2) Bidirectional AC Power Flow: In numerous papers, only (8) and (9) are considered for the energy management of MGs. Although (8) and (9) are fundamental for power flow calculations, they might be insufficient as they do not account for the relationships between currents, voltages, and power flow in MGs. Therefore, (10) and (11) must be added to the formulation, where R_{mn}, X_{mn}, and Z_{mn} represent resistance, reactance, and impedance of line mn, while $\Gamma_{mn,t}$ is a free auxiliary variable. In addition, constraints (12) and (13) ensure that voltages and currents remain within acceptable ranges to prevent damage to devices [45].

$$v^2_{m,t} - v^2_{n,t} = 2\left(R_{mn} p_{mn,t} + X_{mn} q_{mn,t}\right) + Z^2_{mn} i^2_{mn,t} - \Gamma_{mn,t};\ \forall mn \in \Phi_L, \forall t \in \Phi_T \tag{10}$$

$$v^2_{n,t}\ i^2_{mn,t} = \left(p^2_{mn,t} + q^2_{mn,t}\right)\ ;\ \forall mn \in \Phi_L, \forall t \in \Phi_T \tag{11}$$

$$\left(V^{min}_m\right)^2 \le v^2_{m,t} \le \left(V^{\max}_m\right)^2;\ \forall m \in \Phi_N, \forall t \in \Phi_T \tag{12}$$

$$0 \le i^2_{mn,t} \le \left(I^{\max}_{mn}\right)^2;\ \forall mn \in \Phi_L, \forall t \in \Phi_T \tag{13}$$

3) Reconfiguration Model: To model reconfigurability in an MG, it is essential to ensure two sets of constraints. First, it must be guaranteed that no power, either reactive or active, and no current can flow through line mn when the switches for this line are open. Second, it is important to ensure that the MG configuration remains radial after reconfiguration.

In (14), the proper limit for auxiliary variable $\Gamma_{mn,t}$ is considered either zero or the maximum possible square of voltage magnitude rise/drop in the system. Constraint (10) must be replaced by (15) to force the current magnitude in line mn to zero when the line is open. Similarly, inequalities (16) and (17) apply the same logic to power flowing in the line mn. Moreover, the radiality condition is imposed via parent node/child node path as presented in (18)–(20) [46].

$$|\Gamma_{mn,t}| \le \left(\left(V^{\max}_m\right)^2 - \left(V^{min}_m\right)^2\right)\left(1 - \left(y^+_{mn,t} + y^-_{mn,t}\right)\right);\ \forall mn \in \Phi_L, \forall t \in \Phi_T \tag{14}$$

$$i^2_{mn,t} \le \left(I^{\max}_{mn}\right)^2 \left(y^+_{mn,t} + y^-_{mn,t}\right);\ \forall mn \in \Phi_L, \forall t \in \Phi_T \tag{15}$$

$$|p_{mn,t}| \le I^{\max}_{mn} V^{\max}_m \left(y^+_{mn,t} + y^-_{mn,t}\right);\forall mn \in \Phi_L, \forall t \in \Phi_T \tag{16}$$

$$|q_{mn,t}| \le I^{\max}_{mn} V^{\max}_m \left(y^+_{mn,t} + y^-_{mn,t}\right);\forall mn \in \Phi_L, \forall t \in \Phi_T \tag{17}$$

$$\sum_{n|(mn)\in\Phi_L} \left(y^-_{mn,t}\right) + \sum_{n|(nm)\in\Phi_L} \left(y^+_{nm,t}\right) = 1;\ \forall m \in \Phi_N | m \notin \Phi_{PCC}, \forall t \in \Phi_T \tag{18}$$

$$\sum_{n|(mn)\in\Phi_L} \left(y^-_{mn,t}\right) + \sum_{n|(nm)\in\Phi_L} \left(y^+_{nm,t}\right) = 0;\ \forall m \in \Phi_N | m \in \Phi_{PCC}, \forall t \in \Phi_T \tag{19}$$

$$y^+_{mn,t} + y^-_{mn,t} \le 1;\ \forall mn \in \Phi_L, \forall t \in \Phi_T \tag{20}$$

4) Renewable Resources and Distributed Generation: The operation of PV and wind turbine units are defined by (21) and (22), respectively. Where PV and wind actual power injection (non-negative variables $p^{PV}_{pv,t}$ and $p^{W}_{w,t}$) can be calculated in terms of available PV and wind power generation ($\widetilde{P^{PV}_{pv,t}}$ and $\widetilde{P^{W}_{w,t}}$) minus the respective power curtailments (non-negative variables $p^{Cut}_{pv,t}$ and $p^{Cut}_{w,t}$) [44]. The active and reactive power capacity limits of DG units are presented in inequalities (23) and (24) [45].

$$p^{PV}_{pv,t} = \widetilde{P^{PV}_{pv,t}} - p^{Cut}_{pv,t};\ \forall pv \in \Phi_{pv}, \forall t \in \Phi_T \tag{21}$$

$$p^{W}_{w,t} = \widetilde{P^{W}_{w,t}} - p^{Cut}_{w,t};\ \forall w \in \Phi_{w}, \forall t \in \Phi_T \tag{22}$$

$$P^{min}_{dg} \le p^{DG}_{dg,t} \le P^{\max}_{dg};\ \forall dg \in \Phi_{dg}, \forall t \in \Phi_T \tag{23}$$

$$\left|q^{DG}_{dg,t}\right| \le p^{DG}_{dg,t} \tan\left(\cos^{-1}\left(\varphi^{DG}_{dg}\right)\right);\ \forall dg \in \Phi_{dg}, \forall t \in \Phi_T \tag{24}$$

5) Battery Systems: Batteries are critical to the optimal operation of MGs, offering flexibility by storing excess energy during periods of low demand, high electricity prices, or surplus renewable generation. Conversely, during periods of high demand, elevated electricity prices, or reduced renewable generation, batteries can discharge stored energy to balance the MG's power supply and demand. In (25)–(31), battery system charging and discharging model and limits are presented. In (25) and (26), upper bound limits for charging ($p_{b,t}^{C}$) and discharging ($p_{b,t}^{D}$) power of batteries are imposed. The definition of $p_{b,t}^{B}$ based on $p_{b,t}^{C}$ and $p_{b,t}^{D}$ is provided in (27). Accordingly, $p_{b,t}^{B}$ takes a positive value when the battery is in charging mode ($p_{b,t}^{C} > 0$), a negative value in discharging mode ($p_{b,t}^{D} > 0$), and is zero when the battery is idle ($p_{b,t}^{C} = p_{b,t}^{D} = 0$). (28) expresses the complementary condition to ensure that simultaneous charging and discharging cannot occur [47]. Furthermore, (29) and (30) calculate the energy level of the batteries at each time interval based on charging/discharging power and battery efficiency, ensuring that overcharging and deep discharge are prevented as enforced by (31).

$$0 \leq p_{b,t}^{C} \leq P_{b}^{Cmax};\ \forall b \in \Phi_b, \forall t \in \Phi_T \tag{25}$$

$$0 \leq p_{b,t}^{D} \leq P_{b}^{Dmax};\ \forall b \in \Phi_b, \forall t \in \Phi_T \tag{26}$$

$$p_{b,t}^{B} = p_{b,t}^{C} - p_{b,t}^{D};\ \forall b \in \Phi_b, \forall t \in \Phi_T \tag{27}$$

$$p_{b,t}^{C}\, p_{b,t}^{D} = 0;\ \forall b \in \Phi_b, \forall t \in \Phi_T \tag{28}$$

$$e_{b,t}^{B} = E_{b}^{ini} + \Delta_t \left(p_{b,t}^{C} \eta_b^{C} - \frac{p_{b,t}^{D}}{\eta_b^{D}} \right);\forall b \in \Phi_b, \forall t \in \Phi_T | t = 1 \tag{29}$$

$$e_{b,t}^{B} = e_{b,t-1}^{B} + \Delta_t \left(p_{b,t}^{C} \eta_b^{C} - \frac{p_{b,t}^{D}}{\eta_b^{D}} \right); \tag{30}$$
$$\forall b \in \Phi_b, \forall t \in \Phi_T \,|t\rangle\, 1$$

$$E_{b}^{min} \leq e_{b,t}^{B} \leq E_{b}^{\max};\ \forall b \in \Phi_b, \forall t \in \Phi_T \tag{31}$$

C. Day-Ahead Linearized Convex Optimization Model

The developed nonlinear and nonconvex model accurately captures the power flow and optimal operations within RMG. However, it does not ensure the optimality of its solutions and MINLP models for the optimal operation of MGs are typically computationally time-consuming, and a decomposition method may be needed to solve the problem [8]. Consequently, this subsection outlines the process of linearizing the nonlinear model to address these limitations. The first objective function, presented in (1), as well as constraint (8)–(13), (15), and (28) are non-linear. The quadratic function in (1) can be linearized via piecewise linearization as presented in (32)–(34), where maximum discretization blocks of DG's power ($\Delta P_{dg}^{\max}$) and slope in its linearization ($M_{dg,\omega}^{DG}$) can be calculated according to (35) and (36) [48].

$$OF_1 = \min \left(\sum_t \Delta_t \left(\Psi_t^{GRb} p_t^{GRb} - \Psi_t^{GRs} p_t^{GRs} \right) + \left(\sum_t \sum_{dg} \left(\Delta_t p_{dg,t}^{DG} \Psi_{dg}^{b} + \sum_{\omega} \Delta_t{}^2 \left(M_{dg\omega}^{DG} \Delta p_{dg,t,\omega}^{DG} \right) \Psi_{dg}^{C} \right) \right) \right) \tag{32}$$

$$p_{dg,t}^{DG} = \sum_{\omega} \Delta p_{dg,t,\omega}^{DG}\ ;\ \forall dg \in \Phi_{dg}, \forall t \in \Phi_T \tag{33}$$

$$\Delta p_{dg,t,\omega}^{DG} \leq \Delta P_{dg}^{\max};\ \forall dg \in \Phi_{dg}, \forall t \in \Phi_T, \forall \omega \in \Phi_\omega \tag{34}$$

$$\Delta P_{dg}^{\max} = \left(P_{dg}^{\max} - P_{dg}^{min} \right) / \bar{\omega}\ ;\ \forall dg \in \Phi_{dg} \tag{35}$$

$$M_{dg,\omega}^{DG} = (2\omega - 1)\ \Delta P_{dg}^{\max};\ \forall dg \in \Phi_{dg}, \forall \omega \in \Phi_\omega \tag{36}$$

By defining auxiliary non-negative variables $i_{mn,t}^{sqr} = i_{mn,t}^{2}$ and $v_{m,t}^{sqr} = v_{m,t}^{2}$, the nonlinearity in (10), (12), and (15) is resolved. Hence, these constraints are replaced by (37)–(39).

$$v_{m,t}^{sqr} - v_{n,t}^{sqr} = 2\left(R_{mn} p_{mn,t} + X_{mn} q_{mn,t} \right) + Z_{mn}^{2} i_{mn,t}^{sqr} - \Gamma_{mn,t};\ \forall mn \in \Phi_L, \forall t \in \Phi_T \tag{37}$$

$$\left(V_m^{min} \right)^2 \leq v_{m,t}^{sqr} \leq \left(V_m^{\max} \right)^2;\ \forall m \in \Phi_N, \forall t \in \Phi_T \tag{38}$$

$$i_{mn,t}^{sqr} \leq \left(I_{mn}^{\max} \right)^2 \left(y_{mn,t}^{+} + y_{mn,t}^{-} \right);\ \forall mn \in \Phi_L, \forall t \in \Phi_T \tag{39}$$

In constraint (11), by replacing $v_{n,t}^{2}$ on the left-hand side with its estimated value V_n^{Esqr}, and linearizing the squares of the active power ($p_{mn,t}^{2}$) and reactive power ($q_{mn,t}^{2}$) on the right-hand side, a linear constraint (40) is obtained. Slope in piecewise linearization ($M_{dg,\omega}^{PQ}$) can be calculated according to (41). In (42) and (43), auxiliary non-negative variables $p_{mn,t}^{+}$ and $q_{mn,t}^{+}$ represent active and reactive power flowing in the positive direction (from node m to node n), while non-negative variables $p_{mn,t}^{-}$ and $q_{mn,t}^{-}$ represent power flowing in the negative direction (from node n to node m). The relationship between the discretization blocks for active power flowing in line mn ($\Delta p_{mn,t,\omega}$), $p_{mn,t}^{+}$ and $p_{mn,t}^{-}$ is presented in (44). In (45), a similar equation for the discretization blocks for reactive power flowing in line mn ($\Delta q_{mn,t,\omega}$), is expressed. These discretization blocks are limited to their maximum value as imposed via (46) and (47). The value of V_n^{Esqr} and maximum discretization blocks of power ($\Delta p_{mn}^{\max}$ and $\Delta q_{mn}^{\max}$) are calculated according to (48) and (49). Further details and a visual representation of this linearization approach for power flow can be found in [48].

$$V_n^{Esqr}\ i_{mn,t}^{sqr} = \sum_{\omega} M_{mn,\omega}^{PQ} \left(\Delta p_{mn,t,\omega} + \Delta q_{mn,t,\omega} \right)\ ;\ \forall mn \in \Phi_L, \forall t \in \Phi_T \tag{40}$$

$$M_{mn,\omega}^{PQ} = (2\omega - 1)\ \Delta p_{mn}^{\max} = (2\omega - 1)\ \Delta q_{mn}^{\max};\ \forall mn \in \Phi_L, \forall \omega \in \Phi_\omega \tag{41}$$

$$p_{mn,t} = p_{mn,t}^{+} - p_{mn,t}^{-};\ \forall mn \in \Phi_L, \forall t \in \Phi_T \tag{42}$$

$$q_{mn,t} = q_{mn,t}^{+} - q_{mn,t}^{-};\ \forall mn \in \Phi_L, \forall t \in \Phi_T \tag{43}$$

$$\sum_{\omega} \left(\Delta p_{mn,t,\omega} \right) = p_{mn,t}^{+} + p_{mn,t}^{-};\ \forall mn \in \Phi_L, \forall t \in \Phi_T \tag{44}$$

$$\sum_{\omega}\left(\Delta q_{mn,t,\omega}\right)=q^{+}_{mn,t}\ +q^{-}_{mn,t};\ \forall mn\in\Phi_L,\forall t\in\Phi_T \tag{45}$$

$$\Delta p_{mn,t,\omega}\leq\Delta p^{\max}_{mn};\ \forall mn\in\Phi_L,\forall t\in\Phi_T \tag{46}$$

$$\Delta q_{mn,t,\omega}\leq\Delta q^{\max}_{mn};\ \forall mn\in\Phi_L,\forall t\in\Phi_T \tag{47}$$

$$V^{Esqr}_{n}=\left(\left(V^{min}_{n}\right)^2+\left(V^{\max}_{n}\right)^2\right)/2\ ;\ \forall n\in\Phi_N \tag{48}$$

$$\Delta p^{\max}_{mn}=\Delta q^{\max}_{mn}\ =\left(V^{\max}_{m}I^{\max}_{mn}\right)/\bar{\omega}\ ;\ \forall mn\in\Phi_L \tag{49}$$

Non-linear complementary constraint in batteries, presented in (28), can be replaced by a set of linear complementary constraints proposed in [47]. As a result, constraint (28) can be removed and substituted by (50)–(54).

$$\Delta_t p^{C}_{b,t}\leq\left(E^{\max}_{b}-E^{ini}_{b}\right)/\eta^{C}_{b};\ \forall b\in\Phi_b,\forall t\in\Phi_T|t\ =\ 1 \tag{50}$$

$$\Delta_t p^{C}_{b,t}\leq\left(E^{\max}_{b}-e^{B}_{b,t-1}\right)/\eta^{C}_{b};\ \forall b\in\Phi_b,\forall t\in\Phi_T\ |t\rangle\ 1 \tag{51}$$

$$\Delta_t p^{D}_{b,t}\leq\eta^{D}_{b}\ \left(E^{ini}_{b}-E^{min}_{b}\right);\ \forall b\in\Phi_b,\forall t\in\Phi_T|t\ =\ 1 \tag{52}$$

$$\Delta_t p^{D}_{b,t}\leq\eta^{D}_{b}\ \left(e^{B}_{b,t-1}-E^{min}_{b}\right);\ \forall b\in\Phi_b,\forall t\in\Phi_T\ |t\rangle\ 1 \tag{53}$$

$$p^{D}_{b,t}\leq P^{Dmax}_{b}-\left(P^{Dmax}_{b}/P^{Cmax}_{b}\right)p^{C}_{b,t};\ \forall b\in\Phi_b,\forall t\in\Phi_T \tag{54}$$

D. Modeling Assumptions

To clarify the scope and limitations of the proposed formulation, the following key assumptions should be considered:

1) As noted in Section II-C, the original non-linear, non-convex model was reformulated into an MILP model. This involves piecewise linearization of the quadratic cost function for DG units and the non-linear power flow equations. Linearization has been done to guarantee the optimality of solutions and improve computational tractability.
2) It is assumed that MG operator is in charge of making the decisions regarding the scheduling of all DERs in the MG and energy coordination with the main grid. As resilience against the main grid was the focus of the research, the grid-connected operation is deliberately studied.
3) The model always enforces a radial topology for MGs, as described by the constraints in (18)–(20). This is a common assumption for most distribution networks and MGs due to power system protection issues. However, such assumption is not necessary in meshed system.

III. Solution Methodology

This paper proposes a matheuristic approach based on the variable neighborhood descent (VND) algorithm to solve the MILP model (6)–(54). The solution strategy comprises three components: 1) Model adaptations, including slack variables and a penalized objective function, 2) Initial solution generation based on a relaxed MILP model, and 3) Neighborhood structures that allow controlled topology modifications while simultaneously optimizing DG dispatch, storage operation, and energy trading.

A. Modified Model

Neighborhood structures should guarantee feasible solutions, however, due to the operational constraints of the problem, the original formulation could lead to infeasible solutions. In this regard, the positive slack variables $\vartheta^{p+}_{m,t}$, $\vartheta^{p-}_{m,t}$, $\vartheta^{q+}_{m,t}$ and $\vartheta^{q-}_{m,t}$ are included in the power flow balance equations, as presented in (55) and (56). By including these variables, the operational constraints such as voltage, current, GD power dispatch limits of the model are relaxed guaranteeing feasible solutions for the optimization solver in each neighborhood structure. Slack variables are limited according (57) and (58).

$$\begin{aligned}&\sum_{km}p_{km,t}-\sum_{mn}\left(p_{mn,t}+R_{mn}i^2_{mn,t}\right)\\&+\sum_{dg|\ b_{dg}=\ m}p^{DG}_{dg,t}+\sum_{pv|\ b_{pv}=\ m}p^{PV}_{pv,t}+\sum_{wt|\ b_{wt}=\ m}p^{WT}_{wt,t}\\&\quad+p^{GR}_{t}+\vartheta^{p+}_{m,t}-\ \vartheta^{p-}_{m,t}\\&\quad=P^{Load}_{m,t}+\sum_{bs|\ b_{bs}=\ m}p^{BS}_{bs,t};\ \forall m\in\Phi_N,\forall t\in\Phi_T\end{aligned} \tag{55}$$

$$\begin{aligned}&\sum_{km}q_{km,t}-\sum_{mn}\left(q_{mn,t}+X_{mn}i^2_{mn,t}\right)+\sum_{dg|\ b_{dg}=\ m}q^{DG}_{dg,t}\\&\quad+\sum_{rpc|\ b_{rpc}=m}Q^{RPC}_{rpc,t}+q^{GR}_{t}+\vartheta^{q+}_{m,t}-\ \vartheta^{q-}_{m,t}=Q^{Load}_{m,t}\ ;\\&\quad\forall m\in\Phi_N,\forall t\in\Phi_T\end{aligned} \tag{56}$$

$$0\leq\vartheta^{p+}_{m,t},\vartheta^{p-}_{m,t}\leq P^{Load}_{m,t};\ \forall m\in\Phi_N,\forall t\in\Phi_T \tag{57}$$

$$0\leq\vartheta^{q+}_{m,t},\vartheta^{q-}_{m,t}\leq Q^{Load}_{m,t};\ \forall m\in\Phi_N,\forall t\in\Phi_T \tag{58}$$

The slack variables are minimized using a penalization strategy according to (59). Note that penalization parameters should be big enough to ensure slack variables to be zero at the end of the optimization process. Finally, the modified model is presented in (60).

$$f\ =\rho^{p}\sum_{i\in\Phi_N}\sum_{t\in\Phi_T}\left(\vartheta^{p+}_{i,t}+\vartheta^{p-}_{i,t}\right)+\rho^{q}\sum_{i\in\Phi_N}\sum_{t\in\Phi_T}\left(\vartheta^{q+}_{i,t}+\vartheta^{q-}_{i,t}\right); \tag{59}$$

$$minimize OF+f \tag{60}$$

Subject to: (6)–(58).

Note that, since this is a minimization problem, for feasible solutions, slack variables should be zero.

B. Initial Solution

The initial solution approach consists of two sequential stages, described as follows.

The first stage aims to determine an initial value for the integer variables ($y^{+}_{mn,t}$ and $y^{-}_{mn,t}$) that define the topology of the grid. The goal is to obtain a radial configuration while ignoring operational constraints such as voltage and current limits. The initial solution is obtained by solving a simplified version of the proposed model (6)–(60), specifically by omitting constraints (12), (13), and (40)–(49) related to current magnitude calculations. The solution of this simplified model provides a radial topology; however, the operational state of the system is not accurately calculated. At this stage, the current solution of the algorithm is defined by $\hat{y}_{mn,t}$ according to (61), where $\hat{y}_{mn,t} = 1$ for closed circuits and $\hat{y}_{mn,t} = 0$ for the open ones, describing the topology of the grid.

$$\hat{y}_{mn,t} = y^{+}_{mn,t} + y^{-}_{mn,t} \; \forall t \in \Phi_T, \; \forall mn \in \Phi_L \tag{61}$$

In the second stage, the integer variables y^{+}_{ij} and y^{-}_{ij} are fixed in the values determined in the previous stage while omitted constraints are restored to calculate the initial objective function value. Note that this initial solution may be operationally infeasible due voltage and current violations. However, the optimization solver guarantees eventual feasibility through the slack variables ($\vartheta^{p+}_{i,t}$, $\vartheta^{p-}_{i,t}$, $\vartheta^{q+}_{i,t}$, $\vartheta^{q-}_{i,t}$) included into the power flow equations.

Hereinafter the current solution of the algorithm is represented by Y including integer and continuous variables and $OF(Y)$ the objective function value calculated according (60).

C. Neighborhood Structures

The proposed neighborhood structures systematically explore high-quality solutions in the vicinity of the current algorithm solution. These structures allow controlled modifications to the current network topology while simultaneously optimizing: DG power dispatch, batteries operation, and energy trading decisions (buy/sell). Each neighborhood is implemented as a MILP model derived from the modified formulation (6)–(60). In this paper the number of structures is defined by the parameter k. The neighborhood search is guided by two constraints (62) and (63) operating on the current solution of the algorithm Y. Considering the network topology defined by $\hat{y}_{mn,t}$, constraint (62) enforces to close k circuits from the currently open branches.

$$\sum_{(mn)\in\Phi_L |\, \hat{y}_{mn,t}=0,\, \forall t\in\Phi_T} \left(y^{-}_{mn,t} + y^{+}_{mn,t}\right) = k, \tag{62}$$

The auxiliary constraint (63) maintains the operational state of branches not connected to terminal nodes, thereby reducing the search space and computational effort.

$$\begin{aligned} & y^{-}_{mn,t} + y^{+}_{mn,t} = 1, \\ & mn \in \Phi_L, \; \forall t \in \Phi_T |\, \hat{y}_{mn,t} = 1 \wedge m \notin \Phi^N_t \wedge n \notin \Phi^N_t \end{aligned} \tag{63}$$

Where Φ^N_t is the set of nodes that are linked to open circuits at period t.

When incorporated into the modified model (6)–(60), these constraints generate a neighbor solution Y' with exactly $2k$ branches in modified operational states. The resulting MILP model efficiently explores feasible topology variations while maintaining radiality constraints.

Algorithm 1: Pseudo-Code for the Matheuristic Algorithm.

Begin matheuristic algorithm based on VND:
Input Parameters:
- $\bar{k}$: Number neighborhood structures
- Network sets/parameters and time sets from the model
- Objective selector: cost or resilience

Initial solution:
- Solve a relaxed model to determine an initial topology $\hat{y}_{mn,t}$ and a feasible schedule, as presented in Section III-B.
- Use $\hat{y}_{mn,t}$ to compute the initial solution Y and the objective function value $OF(Y)$.
- Set $k \leftarrow 1$
- Determine the set of final nodes Φ_t from $\hat{y}_{mn,t}$

Neighborhood search:
While $k \leq \bar{k}$ to:
  Solve a MILP model to obtain a neighbor solution Y'
   i. If $OF(Y') < OF(Y)$:
    $Y \leftarrow Y'$ (accept improvement)
    $k \leftarrow 1$ (restart from the smallest neighborhood)
    Update Φ_t from the new topology
   ii. Else :
    $k \leftarrow k + 1$ (expand neighborhood scope)

Output:
- Y: Network topology, power trading decisions and operational state of the system

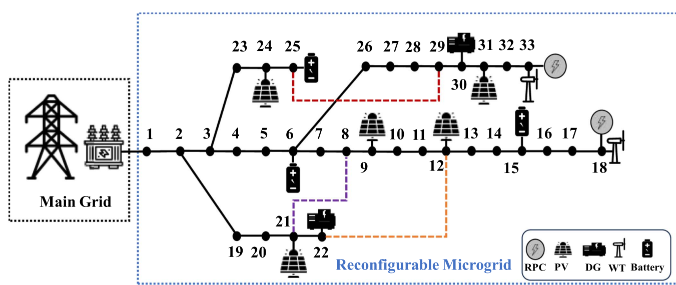

Fig. 2. Schematic diagram of the modified IEEE 33-node system configured as a grid-connected microgrid.

D. Structure of the Proposed Algorithm

The proposed matheuristic structure to solve the proposed MILP model is illustrated in the following pseudocode.

IV. Simulation & Results

The enhanced IEEE 33-bus benchmark test system serves as the base system for the RMGs. As shown in Fig. 2, this system is modified by incorporating several PV (each 600 kW) and WT (each 1500 kW) units, two RPCs, two DG units, and three batteries. Their respective parameters are detailed in Tables II to III. For mathematical optimization, AMPL [49] was used to implement the models, while CPLEX (version 22.1.2) solver [50] and customized VND-based matheuristic algorithm were employed to solve the proposed MILP models. Simulations were performed on a personal computer equipped with an Intel Core

TABLE I
COMPARISON OF THE PROPOSED RESILIENCE-ORIENTED RMG OPERATION MODEL WITH EXISTING LITERATURE

Ref	Reconfiguration	Cost	Resilience	Green resilience	RES	BESS	Multi-objective	Mathematical Model	Solution technique/Solver	Size (bus)
[15]	✓	✓			✓	✓		MILP	CPLEX	10
[16]	✓	✓			✓			MINLP	IPOPT	6, 33
[17]	✓*	✓			✓	✓	✓	NLP	Metaheuristic	Not specified
[18]	✓	✓			✓	✓	✓	MINLP	Metaheuristic	69
[19]	✓*	✓						NLP	Equilibrium Point	12
[20]	✓	✓			✓	✓		MINLP	Heuristic	33
[21]	✓	✓			✓	✓	✓	MINLP	Metaheuristic	33
[22]	✓	✓			✓	✓		MINLP	Metaheuristic	69
[23]	✓	✓			✓	✓	✓	MINLP	DICOPT	10
[24]	✓	✓			✓	✓		MINLP	Metaheuristic	45
[25]	✓	✓			✓			MINLP	Metaheuristic	33
[26]	✓	✓			✓	✓		MILP	Not specified	33
[8]		✓	✓		✓		✓	MINLP	DICOPT	33
[27]		✓	✓		✓	✓		MILP	CPLEX	13
[28]		✓	✓		✓	✓		MILP	Gurobi	Not specified
[29]		✓	✓		✓	✓	✓	MILP	CPLEX	Not specified
[30]		✓	✓		✓	✓		MILP	Not specified	33
[31]			✓		✓	✓		NLP	MOSEK	14, 30, 118
[32]	✓	✓	✓		✓	✓		N/A	Simulink	Not specified
[33]		✓	✓		✓	✓	✓	MINLP	Gurobi	25
[34]		✓	✓		✓	✓	✓	MILP	Gurobi	33
[35]		✓	✓		✓	✓		MILP	CPLEX	Not specified
[37]	✓	✓	✓		✓	✓		MINLP	Not specified	14, 55
[38]	✓	✓	✓		✓	✓	✓	MILP	Gurobi	33
[39]	✓	✓	✓		✓	✓		MILP	COIN-OR	6
[40]	✓	✓			✓	✓		MILP	CPLEX	33
This study	✓	✓	✓	✓	✓	✓	✓	MILP	Matheuristic	33

* The reconfiguration is considered but not directly in an optimization model.

TABLE II
PARAMETERS OF DG UNITS

Unit	Bus	Λ_{dg}^{b} [USD/kWh]	Λ_{dg}^{c} [USD/(kWh)2]	P_{dg}^{max} [kW]	P_{dg}^{min} [kW]	φ_{dg}^{DG}
DG 1	22	0.10	0.0001	1000	50	0.9
DG 2	30	0.09	0.0002	1000	50	0.9

TABLE III
PARAMETERS OF BATTERIES

Unit	Bus	E_{bs}^{max} [kWh]	E_{bs}^{min} [kWh]	P_{bs}^{Chmax} [kW]	P_{bs}^{Chmin} [kW]	η_{bs}^{Ch}	η_{bs}^{Di}
Battery 1	6	500	50	200	100	0.90	0.85
Battery 2	15	500	50	150	150	0.90	0.85
Battery 3	25	500	50	100	120	0.90	0.85

i7-6500U CPU @2.50 GHz and 8 GB RAM, running Windows 10 64-bit. Overview of simulation scenarios presented in Fig. 3.

A. Case I: Cost Minimization Model (CPLEX Vs Matheuristic)

The purpose of this case study is to compare the computational time between the conventional method (CPLEX) and the proposed matheuristic algorithm. In this scenario, the objective function is the total cost, which is minimized. When solved using CPLEX, the total cost of the RMG is $5,297.71, with total PV and WT energy generation over the 24-hour simulation horizon of 17,510.40 kWh and 33,425.10 kWh, respectively. The total energy imported from the main grid is 31,545.23 kWh, and the total computational time (i.e., total solve elapsed time) is 1,629.74 seconds. Using the proposed matheuristic method, the total cost of the RMG is $5,300.35, indicating a negligible difference compared to the conventional approach. The total PV and WT energy generation remain unchanged at 17,510.40 kWh and 33,425.10 kWh, respectively. However, the computational time is significantly reduced with the proposed method, requiring only 103.32 seconds. The hourly PV and WT power generation profiles are illustrated in Fig. 4 . The lower computational time can be explained by the nature of the proposed matheuristic framework. The algorithm explores diverse neighborhoods to avoid local optima, while the MILP solver solves subproblems within each neighborhood. This dual mechanism guarantees that solution spaces are properly explored and exploited with mathematical rigor. Hence, the proposed matheuristic reaches a balance between solution quality and computational efficiency.

B. Case II: Resilience Maximization Model (IPI Vs GIPI)

The purpose of this case study is to compare the proposed resilience index, GIPI, with IPI from both resiliency and sustainability perspectives. In this case, resilience maximization is performed separately for both IPI and GIPI as resilience indices.

IPI: The maximum IPI of the RMG is 0.945, obtained using the CPLEX solver, with a total computational time of only 30.13 seconds considerably faster than in Case I, where cost minimization was the objective. As shown in Fig. 4, the total PV and WT energy generation over the 24-hour simulation horizon are 15,132.90 kWh and 25,038.23 kWh, respectively, indicating 13.58% and 25.09% renewable energy curtailment compared to Case I. The total energy imported from the main grid is 4651.99 kWh, representing an 85.30% reduction compared to Case I.

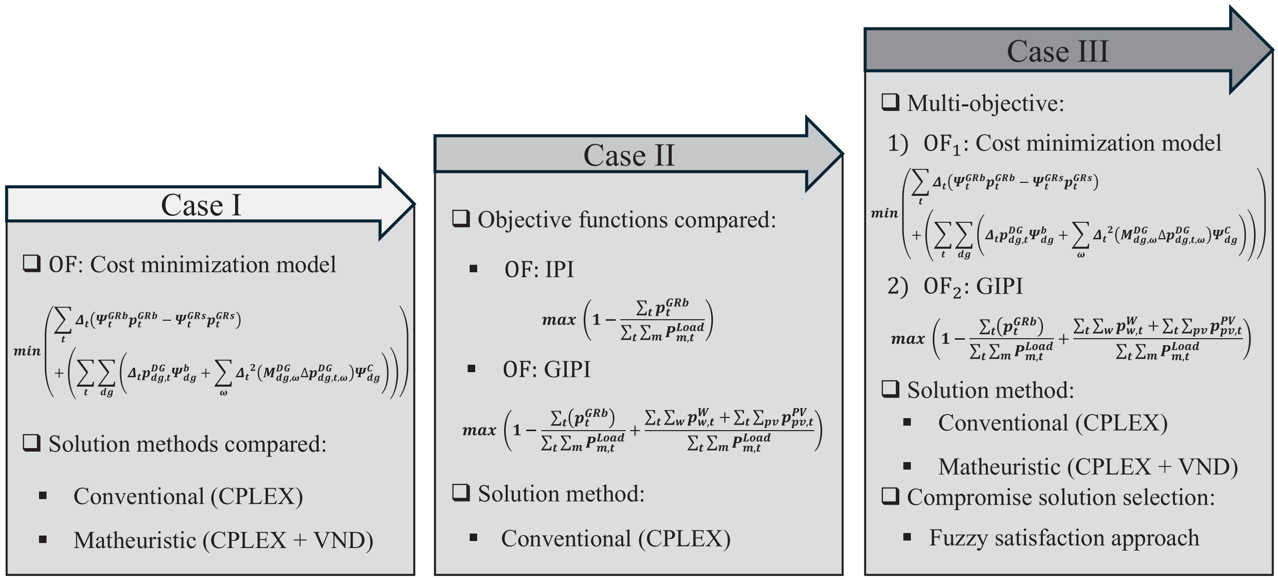

Fig. 3. Overview of simulation scenarios concerning objective functions and solution methods across case studies.

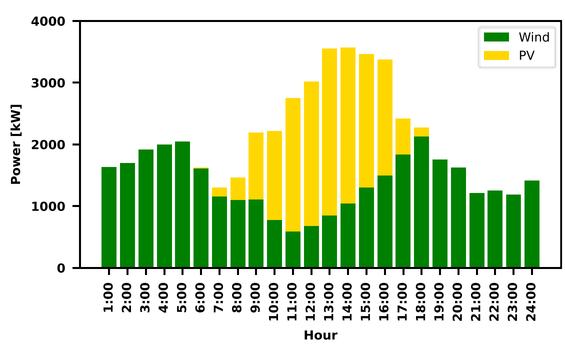

Fig. 4. Power generation of WT and PV units in Case I.

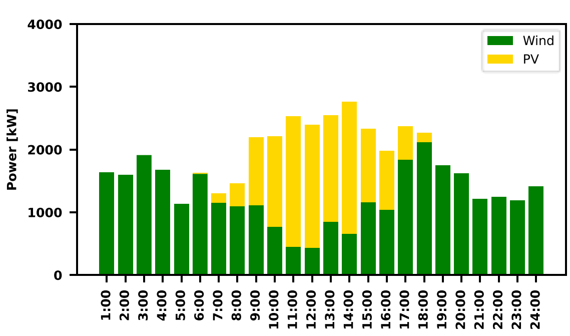

Fig. 5. Total power generation of WT and PV units in Case II using IPI as the resilience index.

GIPI: The maximum GIPI of the RMG is 1.541, also obtained using the CPLEX solver. Similar to IPI, the total computational time is low, at 42.28 seconds, which is significantly faster than in Case I. The total PV and WT energy generation over the 24-hour simulation horizon are 13,644.77 kWh and 30,725.15 kWh, respectively, showing no renewable energy curtailment compared

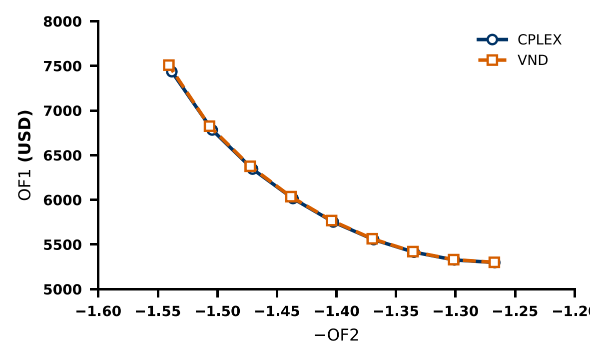

Fig. 6. Pareto curve multi-objective model in Case III.

to Case I. The total energy imported from the main grid is 4,702.87 kWh, representing an 85.13% reduction compared to Case I, and a 1.09% increase compared to IPI. Therefore, the results indicate that while the IPI index enhances the resilience of the RMG by increasing its independence from the main grid, it may also result in higher renewable energy curtailment. In contrast, the proposed GIPI metric achieves the same resilience benefits by improving the independence of the RMG, without causing any reduction in renewable energy generation. Thus, GIPI maintains the resilience advantage of IPI while avoiding renewable energy curtailment.

These differences can be explained by the way each resilience index influences the optimization process. Under the IPI metric, the objective strictly rewards reducing grid imports but does not account for renewable energy curtailment. To maximize the IPI, the optimization increases the dispatch of DGs, since this directly reduces reliance on the main grid. However, the additional DG generation alters power flows and may lead to technical constraints such as voltage rise, line thermal congestion, or reverse power flow, particularly in feeders with high renewable

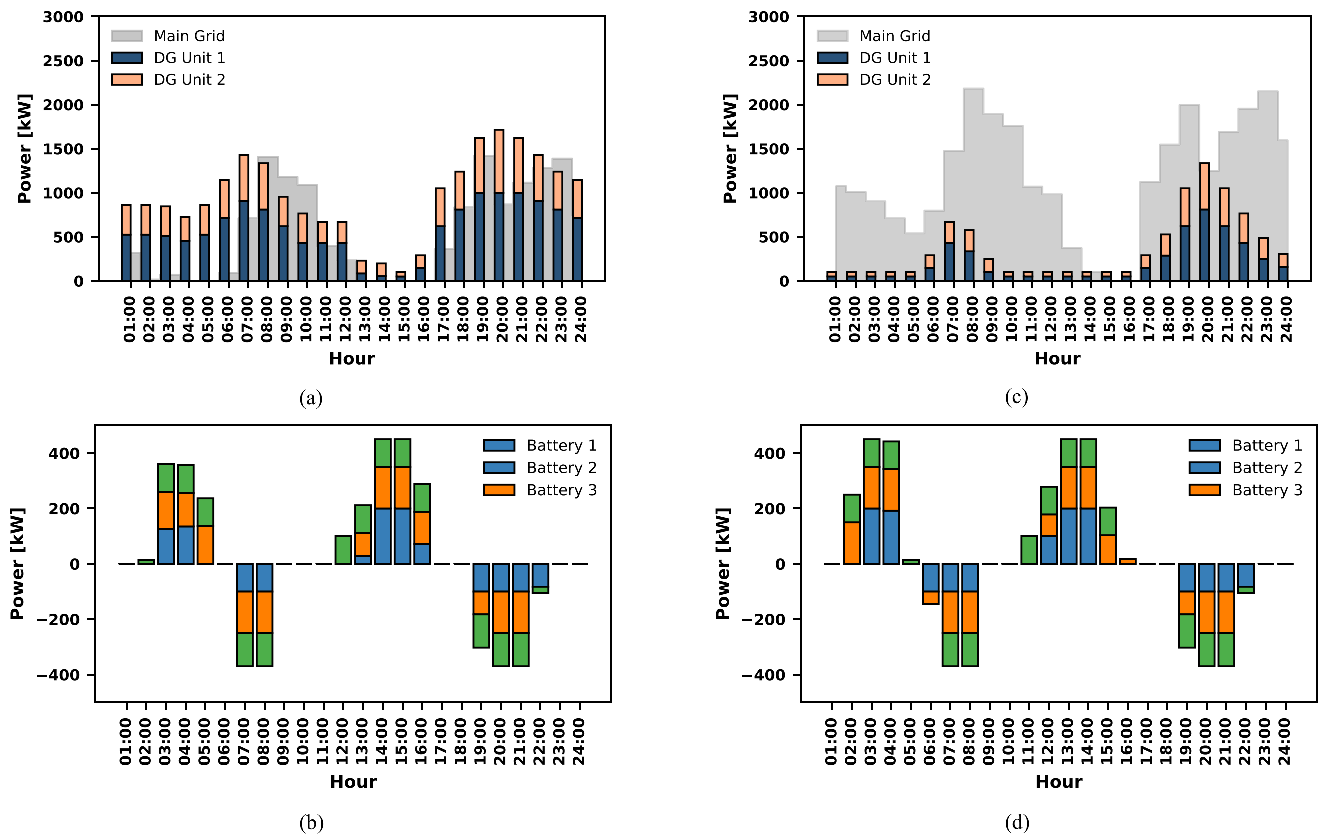

Fig. 7. (a) Scheduled active power of generators for the compromise solution; (b) Charging and discharging power of batteries for the compromise solution; (c) Scheduled active power of generators for cost minimization; (d) Charging and discharging power of batteries for cost minimization.

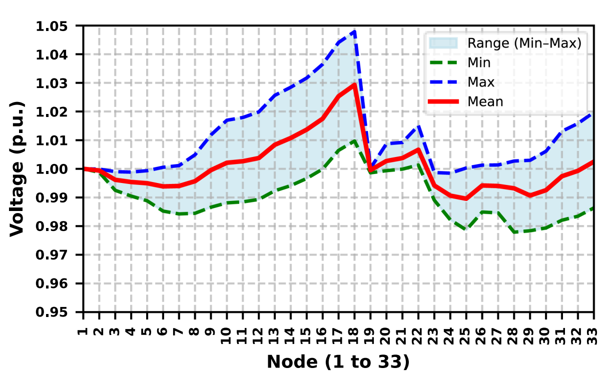

Fig. 8. Voltage range across nodes (best compromise Solution).

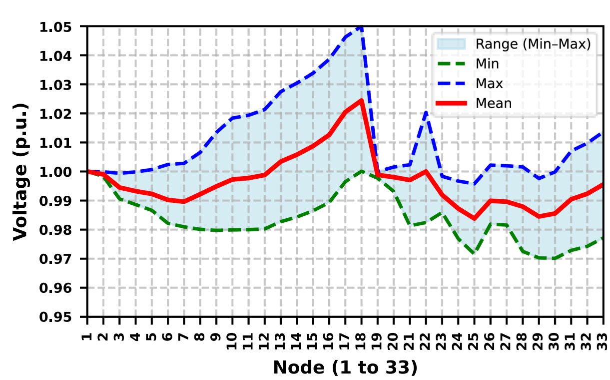

Fig. 9. Voltage range across nodes (cost minimization solution).

penetration. These constraints ultimately force the model to curtail part of the available PV and WT generation. In contrast, the proposed GIPI incorporates renewable utilization explicitly into the resilience objective resulting in more balanced scheduling of DGs and batteries enabling the system to accommodate local PV and wind resources without violating network constraints. Consequently, the GIPI-based operation attains resilience levels comparable to IPI while avoiding unnecessary renewable curtailment and thereby improving overall sustainability.

C. Case III: Multi-objective Model Pareto Front (CPLEX Vs Matheuristic)

The purpose of this case study is to obtain the Pareto front and the best compromise solution for the proposed multi-objective model using the VND and CPLEX algorithms. The ε-constraint method and the fuzzy satisfaction approach are employed to generate the Pareto-optimal set and to select the best compromise solution, respectively [51].

The Pareto fronts for the proposed multi-objective model are presented in Fig. 6. As shown in Fig. 6, both VND and CPLEX yield similar Pareto fronts. However, their computational times differ significantly: 959.58 seconds for the proposed VND-based matheuristic versus 18,261.91 seconds for CPLEX solver, making the conventional method an inappropriate option for this multi-objective problem. The Pareto front ranges from cost minimization toward only GIPI maximization. According to Fig. 6, enhancement in one objective function results in a decline in the performance of the other, due to the inherent conflict between the objectives. The tradeoff observed in the Pareto front is due to the fundamental conflict between economic cost minimization and resilience maximization. In the cost minimization solution, the system relies more heavily on cheaper energy imported from the main grid, while local DG units operate close to their minimum output. This change in the scheduling lowers total operating cost but also increases dependency on the main grid. In the compromise solution, the model deliberately increases DG generation, even during hours when grid power is less expensive, because doing so enhances the GIPI index by reducing reliance on external supply.

To select the well-balanced solution, the fuzzy satisfaction approach can be used. In this method, fuzzy membership functions are constructed for each objective based on the results of the ε-constraint technique. The final compromise solution is then determined by evaluating the intersection of these membership functions. The best compromise solution, based on the Pareto front and deploying fuzzy satisfaction method, corresponds to OF1 = \$6,035.62 and OF2 (i.e., GIPI) = 1.43. The total cost of the best compromise solution shows a 13.87% increase compared to the optimal cost minimization solution (i.e., Case I), which is \$5,300.35. This increase is attributable to the higher operational cost associated with increased DG generation as it can be seen in Fig. 7(a)–(d). These subfigures present the scheduled active power of DG units, imported power from the main grid, and the charging/discharging power profiles of batteries under two distinct optimization solutions: the compromise solution and the cost minimization solution. Fig. 7(a) and (b) correspond to the compromise solution, while Fig. 7(c) and (d) are associated with the total cost minimization solution. Contrasting Fig. 7(a) and (c) shows that DG units contribute considerably more power to the RMG in all the time intervals to reduce the dependency on the main grid and increase the GIPI resilience index. As a result, power imported from the main grid is significantly declined, placing the RMG in a more autonomous operational state. For instance, according to Fig. 7(c), between 00:00 and 05:00, DG units play a marginal role in supplying the demand by generating the minimum power. In contrast, by considering Fig. 7(a), the DG generation between 00:00 and 05:00 considerably increased, while contrasting Fig. 7(b) and (d) shows that the pattern of charging of batteries is also changed during this time interval and less energy stored to help to reduce the power imported from the main grid. A similar pattern is observable between 09:00 and 16:00, where DG units have marginal role for power generation as shown in Fig. 7(c), while they generate more power during the same time interval to increase the GIPI as depicted in Fig. 7(a). The voltage range for the best compromise solution and the optimal cost minimization solution are shown in Figs. 8 and 9, respectively. Contrasting these figures indicates that the voltage range is narrower in the best compromise solution compared to the cost minimization solution, although both remain within the acceptable 5% deviation range (0.95-1.05). In addition, according to Fig. 9, voltages at nodes 29 and 30 reach 0.97 p.u., whereas the minimum voltage in the compromise solution is approximately 0.98 p.u. This demonstrates that increased DG generation leads to an improved voltage profile. The optimal 12 configurations, with one configuration for each two-hour interval, are presented in Table IV, showing the switching status of normally closed and normally open (i.e., tie-line) switches in the RMG. As radiality must be maintained in the RMG, exactly three lines can be open in each configuration. According to Table IV, the configuration of the RMG remains unchanged from 08:00 to 18:00 for the best compromise solution showing less configuration variation compared to the cost minimization solution.

TABLE IV
RECONFIGURATION OF RMG IN CASE III (COMPROMISE SOLUTION)

Time	Open lines (node–node) (best compromise Solution)	Open lines (node–node) (cost minimization solution)
00:00-02:00	27–28, 8–21, 12–22	20–21, 28–29, 8–21
02:00-04:00	5–6, 6–26, 8–21	20–21, 27–28, 8–21
04:00-06:00	27–28, 8–21, 12–22	19–20, 28–29, 12–22
06:00-08:00	6–7, 27–28, 12–22	7–8, 28–29, 12–22
08:00-10:00	28–29, 8–21, 12–22	28–29, 8–21, 12–22
10:00-12:00	28–29, 8–21, 12–22	8–21, 12–22, 25–29
12:00-14:00	28–29, 8–21, 12–22	21–22, 24–25, 8–21
14:00-16:00	28–29, 8–21, 12–22	21–22, 28–29, 8–21
16:00-18:00	28–29, 8–21, 12–22	28–29, 8–21, 12–22
18:00-20:00	19–20, 28–29, 12–22	6–7, 27–28, 12–22
20:00-22:00	6–7, 8–9, 28–29	7–8, 28–29, 12–22
22:00-24:00	19–20, 28–29, 12–22	20–21, 28–29, 12–22

It is worth noting that the proposed model is flexible and can be applied to any number of reconfigurations, ranging from one per hour to a single reconfiguration for the entire day. However, increasing the number of reconfigurations results in a higher number of switching operations and greater computational time.

V. CONCLUSION

This paper presents a comprehensive and scalable approach for the resilience-oriented operation of renewable-powered reconfigurable microgrids (RMGs). The Green Independence Performance Index (GIPI) was introduced as a novel resilience metric to ensure that microgrids can maximize their independence from the main grid while fully utilizing available renewable resources and avoiding renewable energy curtailment. To balance sustainability and economic operation, a multi-objective optimization model was developed to simultaneously minimize total operational costs and maximize GIPI. Recognizing the computational complexity of the original nonlinear and non-convex formulation, the model was reformulated as a mixed-integer linear programming (MILP) problem using piecewise linearization and approximation techniques, ensuring tractability and global optimality. To further improve computational efficiency, a custom matheuristic algorithm was developed, combining classical optimization with heuristic search to achieve high-quality solutions in significantly reduced time frames. Numerical experiments on the enhanced IEEE 33-bus test system demonstrated the effectiveness of the proposed approach in eliminating renewable curtailment, achieving near-optimal operational costs, and significantly reducing computational burden compared to conventional solvers. Future work could incorporate other energy vectors such as hydrogen, thermal energy (heating and cooling), and power-to-X technologies into the RMG framework. Uncertainty modeling was not the focus of this paper; however, the proposed MILP model can be naturally extended in future work to incorporate uncertainty using methods such as fuzzy programming, information gap decision theory, or robust optimization.

References

[1] J. Sora, I. Serban, and D. Petreus, "Enhancing microgrid operation through electric vehicle integration: A survey," *IEEE Access*, vol. 12, pp. 64897–64912, 2024, doi: 10.1109/ACCESS.2024.3397587.

[2] M. Uddin, H. Mo, D. Dong, S. Elsawah, J. Zhu, and J. M. Guerrero, "Microgrids: A review, outstanding issues and future trends," *Energy Strateg. Rev.*, vol. 49, 2023, Art. no. 101127, doi: 10.1016/j.esr.2023.101127.

[3] L. Chen, L. Gao, S. Xing, Z. Chen, and W. Wang, "Zero-carbon microgrid: Real-world cases, trends, challenges, and future research prospects," *Renewable Sustain. Energy Rev.*, vol. 203, 2024, Art. no. 114720, doi: 10.1016/j.rser.2024.114720.

[4] A. Younesi, H. Shayeghi, Z. Wang, P. Siano, A. Mehrizi-Sani, and A. Safari, "Trends in modern power systems resilience: State-of-the-art review," *Renewable Sustain. Energy Rev.*, vol. 162, 2022, Art. no. 112397.

[5] S. F. Zandrazavi and M. Shafie-Khah, "Resilient energy management of networked microgrids and renewable energy resource," in *Future Modern Distribution Networks Resilience*. Amsterdam, The Netherlands; New York, NY, USA: Elsevier, 2024, pp. 279–302.

[6] T. E. K. Zidane et al., "Power systems and microgrids resilience enhancement strategies: A review," *Renewable Sustain. Energy Rev.*, vol. 207, 2025, Art. no. 114953, doi: 10.1016/j.rser.2024.114953.

[7] M. S. Miah, R. Shah, N. Amjady, T. Surinkaew, and S. Islam, "Resiliency assessment and enhancement of renewable dominated edge of grid under high-impact low-probability events—A review," *IEEE Trans. Ind. Appl.*, vol. 60, no. 5, pp. 7578–7598, Sep./Oct. 2024.

[8] V. Shahbazbegian, M. Shafie-khah, H. Laaksonen, G. Strbac, and H. Ameli, "Resilience-oriented operation of microgrids in the presence of power-to-hydrogen systems," *Appl. Energy*, vol. 348, Oct. 2023, Art. no. 121429, doi: 10.1016/J.APENERGY.2023.121429.

[9] H. Karimi and S. Jadid, "Optimal energy management for multi-microgrid considering demand response programs: A stochastic multi-objective framework," *Energy*, vol. 195, 2020, Art. no. 116992, doi: 10.1016/j.energy.2020.116992.

[10] X. Liang, M. A. Saaklayen, M. A. Igder, S. M. R. H. Shawon, S. O. Faried, and M. Janbakhsh, "Planning and service restoration through microgrid formation and soft open points for distribution network modernization: A review," *IEEE Trans. Ind. Appl.*, vol. 58, no. 2, pp. 1843–1857, Mar./Apr. 2022, doi: 10.1109/TIA.2022.3146103.

[11] R. Vargas, L. H. Macedo, J. M. Home-Ortiz, J. R. S. Mantovani, and R. Romero, "Optimal restoration of active distribution systems with voltage control and closed-loop operation," *IEEE Trans. Smart Grid*, vol. 12, no. 3, pp. 2295–2306, May 2021, doi: 10.1109/TSG.2021.3050931.

[12] S. Thakar, A. S. V., and S. Doolla, "System reconfiguration in microgrids," *Sustain. Energy, Grids Netw.*, vol. 17, 2019, Art. no. 100191, doi: 10.1016/j.segan.2019.100191.

[13] C. L. B. Silveira, A. Tabares, L. T. Faria, and J. F. Franco, "Mathematical optimization versus metaheuristic techniques: A performance comparison for reconfiguration of distribution systems," *Electr. Power Syst. Res.*, vol. 196, 2021, Art. no. 107272.

[14] M. A. Boschetti and V. Maniezzo, "Matheuristics: Using mathematics for heuristic design," *4OR*, vol. 20, no. 2, pp. 173–208, 2022.

[15] M. Hemmati, B. Mohammadi-Ivatloo, M. Abapour, and A. Anvari-Moghaddam, "Optimal chance-constrained scheduling of reconfigurable microgrids considering islanding operation constraints," *IEEE Syst. J.*, vol. 14, no. 4, pp. 5340–5349, Dec. 2020, doi: 10.1109/JSYST.2020.2964637.

[16] A. Jahani, K. Zare, L. M. Khanli, and H. Karimipour, "Optimized power trading of reconfigurable microgrids in distribution energy market," *IEEE Access*, vol. 9, pp. 48218–48235, 2021, doi: 10.1109/ACCESS.2021.3064634.

[17] K. Thirugnanam, M. S. El Moursi, V. Khadkikar, H. H. Zeineldin, and M. A. Hosani, "Energy management strategy of a reconfigurable grid-tied hybrid AC/DC microgrid for commercial building applications," *IEEE Trans. Smart Grid*, vol. 13, no. 3, pp. 1720–1738, May 2022, doi: 10.1109/TSG.2022.3141459.

[18] F. Yin et al., "A secured social-economic framework based on PEM-blockchain for optimal scheduling of reconfigurable interconnected microgrids," *IEEE Access*, vol. 9, pp. 40797–40810, 2021, doi: 10.1109/ACCESS.2021.3065400.

[19] Q. Zhou, M. Shahidehpour, A. Alabdulwahab, and A. Abusorrah, "Privacy-preserving distributed control strategy for optimal economic operation in islanded reconfigurable microgrids," *IEEE Trans. Power Syst.*, vol. 35, no. 5, pp. 3847–3856, Sep. 2020, doi: 10.1109/TPWRS.2020.2985995.

[20] M. Dabbaghjamanesh, A. Kavousi-Fard, and J. Zhang, "Stochastic modeling and integration of plug-In hybrid electric vehicles in reconfigurable microgrids with deep learning-based forecasting," *IEEE Trans. Intell. Transp. Syst.*, vol. 22, no. 7, pp. 4394–4403, Jul. 2021, doi: 10.1109/TITS.2020.2973532.

[21] L. J. Varghese, U. A. Kumar, and D. Sunitha, "Solar PV and wind energy based reconfigurable microgrid for optimal load dispatch," *J. Electr. Eng. Technol.*, vol. 18, no. 4, pp. 2909–2928, 2023.

[22] M. Hemmati, B. Mohammadi-Ivatloo, M. Abapour, and A. Anvari-Moghaddam, "Day-ahead profit-based reconfigurable microgrid scheduling considering uncertain renewable generation and load demand in the presence of energy storage," *J. Energy Storage*, vol. 28, 2020, Art. no. 101161.

[23] M. Hemmati et al., "Economic-environmental analysis of combined heat and power-based reconfigurable microgrid integrated with multiple energy storage and demand response program," *Sustain. Cities Soc.*, vol. 69, 2021, Art. no. 102790, doi: 10.1016/j.scs.2021.102790.

[24] M. Elgamal, N. Korovkin, A. Abdel Menaem, and A. Elmitwally, "Day-ahead complex power scheduling in a reconfigurable hybrid-energy islanded microgrid with responsive demand considering uncertainty and different load models," *Appl. Energy*, vol. 309, 2022, Art. no. 118416, doi: 10.1016/j.apenergy.2021.118416.

[25] S. Thakar, A. S. Vijay, and S. Doolla, "Effect of P-Q limits on microgrid reconfiguration: A capability curve perspective," *IEEE Trans. Sustain. Energy*, vol. 11, no. 3, pp. 2040–2048, Jul. 2020, doi: 10.1109/TSTE.2019.2952043.

[26] M. Dabbaghjamanesh, A. Kavousi-Fard, S. Mehraeen, J. Zhang, and Z. Y. Dong, "Sensitivity analysis of renewable energy integration on stochastic energy management of automated reconfigurable hybrid AC–DC microgrid considering DLR security constraint," *IEEE Trans. Ind. Informat.*, vol. 16, no. 1, pp. 120–131, Jan. 2020, doi: 10.1109/TII.2019.2915089.

[27] J. A. A. Silva, J. C. López, N. B. Arias, M. J. Rider, and L. C. P. da Silva, "An optimal stochastic energy management system for resilient microgrids," *Appl. Energy*, vol. 300, 2021, Art. no. 117435, doi: 10.1016/j.apenergy.2021.117435.

[28] H. Masrur, M. M. Gamil, M. R. Islam, K. M. Muttaqi, M. S. H. Lipu, and T. Senjyu, "An optimized and outage-resilient energy management framework for multicarrier energy microgrids integrating demand response," *IEEE Trans. Ind. Appl.*, vol. 58, no. 3, pp. 4171–4180, May/Jun. 2022, doi: 10.1109/TIA.2022.3160683.

[29] B. Ahmadisourenabadi, M. Marzband, S. Hosseini-Hemati, S. M. B. Sadati, and A. Rastgou, "Quantifying and enabling the resiliency of a microgrid considering electric vehicles using a bayesian network risk assessment," *Energy*, vol. 308, no. April, 2024, Art. no. 133036, doi: 10.1016/j.energy.2024.133036.

[30] W. Cao and L. Zhou, "Resilient microgrid modeling in digital twin considering demand response and landscape design of renewable energy," *Sustain. Energy Technol. Assessments*, vol. 64, 2024, Art. no. 103628, doi: 10.1016/j.seta.2024.103628.

[31] M. Isfakul Anam, T.-T. Nguyen, and T. Vu, "Risk-based preventive energy management for resilient microgrids," *Int. J. Electr. Power Energy Syst.*, vol. 154, 2023, Art. no. 109391, doi: 10.1016/j.ijepes.2023.109391.

[32] J. Lee, G. Razeghi, and S. Samuelsen, "Utilization of battery electric buses for the resiliency of islanded microgrids," *Appl. Energy*, vol. 347, 2023, Art. no. 121295, doi: 10.1016/j.apenergy.2023.121295.

[33] D. Tang et al., "Economic and resilience-oriented operation of coupled hydrogen-electricity energy systems at ports," *Appl. Energy*, vol. 390, 2025, Art. no. 125825, doi: 10.1016/j.apenergy.2025.125825.

[34] H. Hematian, M. T. Askari, M. A. Ahmadi, M. Sameemoqadam, and M. B. Nik, "Robust optimization for microgrid management with compensator, EV, storage, demand response, and renewable integration," *IEEE Access*, vol. 12, pp. 73413–73425, 2024, doi: 10.1109/ACCESS.2024.3401834.

[35] M. MansourLakouraj, M. J. Sanjari, M. S. Javadi, M. Shahabi, and J. P. S. Catalão, "Exploitation of microgrid flexibility in distribution system hosting prosumers," *IEEE Trans. Ind. Appl.*, vol. 57, no. 4, pp. 4222–4231, Jul./Aug. 2021, doi: 10.1109/TIA.2021.3073882.

[36] M. A. Igder, X. Liang, and M. Mitolo, "Service restoration through microgrid formation in distribution networks: A review," *IEEE Access*, vol. 10, pp. 46618–46632, 2022, doi: 10.1109/ACCESS.2022.3171234.

[37] L. Jia, S. Pannala, G. Kandaperumal, and A. Srivastava, "Coordinating energy resources in an islanded microgrid for economic and resilient operation," *IEEE Trans. Ind. Appl.*, vol. 58, no. 3, pp. 3054–3063, May/Jun. 2022, doi: 10.1109/TIA.2022.3154337.

[38] A. Niknami, M. Tolou Askari, M. Amir Ahmadi, M. Babaei Nik, and M. Samiei Moghaddam, "Resilient day-ahead microgrid energy management with uncertain demand, EVs, storage, and renewables," *Clean. Eng. Technol.*, vol. 20, 2024, Art. no. 100763, doi: 10.1016/j.clet.2024.100763.

[39] A. D. Bintoudi and C. Demoulias, "Optimal isolated microgrid topology design for resilient applications," *Appl. Energy*, vol. 338, 2023, Art. no. 120909, doi: 10.1016/j.apenergy.2023.120909.

[40] S. F. Zandrazavi and M. Shafie-khah, "Optimal operation of PV-integrated reconfigurable microgrids and computational burden," in *Proc. IEEE Int. Conf. Environ. Elect. Eng. 2024 IEEE Ind. Commercial Power Syst. Europe*, 2024, pp. 1–6.

[41] H. Karimi and S. Jadid, "Optimal energy management for multi-microgrid considering demand response programs: A stochastic multi-objective framework," *Energy*, vol. 195, Mar. 2020, Art. no. 116992, doi: 10.1016/J.ENERGY.2020.116992.

[42] T. Abedi, G. Yousefi, and M. Shafie-Khah, "Hierarchical stochastic frequency constrained micro-market model for isolated microgrids," *IEEE Trans. Smart Grid*, vol. 15, no. 1, pp. 5–18, Jan. 2024, doi: 10.1109/TSG.2023.3266761.

[43] Y. Gupta, R. Nellikkath, K. Chatterjee, and S. Doolla, "Volt-var optimization and reconfiguration: Reducing power demand and losses in a droop-based microgrid," *IEEE Trans. Ind. Appl.*, vol. 57, no. 3, pp. 2769–2781, May/Jun. 2021, doi: 10.1109/TIA.2021.3057008.

[44] S. F. Zandrazavi, C. P. Guzman, A. T. Pozos, J. Quiros-Tortos, and J. F. Franco, "Stochastic multi-objective optimal energy management of grid-connected unbalanced microgrids with renewable energy generation and plug-in electric vehicles," *Energy*, vol. 241, 2022, Art. no. 122884.

[45] J. M. Home-Ortiz, L. H. Macedo, R. Vargas, R. Romero, J. R. S. Mantovani, and J. P. S. Catalao, "Increasing RES hosting capacity in distribution networks through closed-loop reconfiguration and volt/VAr control," *IEEE Trans. Ind. Appl.*, vol. 58, no. 4, pp. 4424–4435, Jul./Aug. 2022, doi: 10.1109/TIA.2022.3177175.

[46] R. A. Jabr, R. Singh, and B. C. Pal, "Minimum Loss network reconfiguration using mixed-integer convex programming," *IEEE Trans. Power Syst.*, vol. 27, no. 2, pp. 1106–1115, May 2012, doi: 10.1109/TPWRS.2011.2180406.

[47] D. Pozo, "Linear battery models for power systems analysis," *Electr. Power Syst. Res.*, vol. 212, Nov. 2022, Art. no. 108565, doi: 10.1016/J.EPSR.2022.108565.

[48] S. F. Zandrazavi, A. T. Pozos, J. F. Franco, and M. Shafie-khah, "Planning the operation and expansion of power distribution systems considering electric vehicles (smart charging)," in *Advanced Technologies in Electric Vehicles*. Amsterdam, The Netherlands: Elsevier, 2024, pp. 259–277.

[49] R. Fourer, D. M. Gay, and B. W. Kernighan, "AMPL: A mathematical programming language," *Manage. Sci.*, vol. 36, no. 5, pp. 519–554, 1990.

[50] R. Anand, D. Aggarwal, and V. Kumar, "A comparative analysis of optimization solvers," *J. Statist. Manage. Syst.*, vol. 20, no. 4, pp. 623–635, 2017.

[51] S. Nojavan, M. Majidi, A. Najafi-Ghalelou, M. Ghahramani, and K. Zare, "A cost-emission model for fuel cell/PV/battery hybrid energy system in the presence of demand response program: ε-constraint method and fuzzy satisfying approach," *Energy Convers. Manage.*, vol. 138, pp. 383–392, 2017, doi: 10.1016/j.enconman.2017.02.003.